Active Flow Separation Control on a NACA 0015 Wing using Fluidic Actuators

LaTunia Pack Melton*

NASA Langley Research Center, Hampton, Virginia, United States of America

Results are presented from a recent set of wind tunnel experiments using sweeping jet actuators to control flow separation on the 30% chord trailing edge flap of a 30° swept wing model with an aspect ratio (AR) of 4.35. Two sweeping jet actuator locations were examined, one on the flap shoulder and one on the trailing edge flap. The parameters that were varied included actuator momentum, freestream velocity, and trailing edge flap deflection (δ_f) angle. The primary focus of this set of experiments was to determine the mass flow and momentum requirements for controlling separation on the flap, especially at large flap deflection angles which would be characteristic of a high lift system. Surface pressure data, force and moment data, and stereoscopic particle image velocimetry (PIV) data were acquired to evaluate the performance benefits due to applying active flow control. Improvements in lift over the majority of the wing span were obtained using sweeping jet actuator control. High momentum coefficient, C_μ, levels were needed when using the actuators on the flap because they were located downstream of separation. Actuators on the flap shoulder performed slightly better but actuator size, orientation, and spacing still need to be optimized.

Nomenclature

b	wing span
c	airfoil chord measured perpendicular to the leading edge (at $\delta_f = 0^o$)
C_L	lift coefficient
C_μ	SWJ actuator momentum coefficient, $\dot{m}U_{jet}/(S_{ref}q)$
$C_{\mu,z}$	ZNMF actuator momentum coefficient, $\equiv J^{'}/cq$
C_p	normalized pressure coefficient, $\equiv (C_{p,sw}/cos^2(\Lambda')$
$C_{p,sw}$	pressure coefficient, $\equiv (P - P_s)/q$
ΔC_L	lift increment
f	frequency, Hz
F^+	reduced frequency, $\equiv (fx_{sp})/U_\infty$
h	slot height, mm
J'	oscillatory momentum at slot exit, $\equiv \rho h u_{p,j}^2$
M	freestream Mach number
$\dot{m}$	mass flow rate, $\rho V Area$
P	pressure
P_s	tunnel static pressure
q	freestream dynamic pressure, $\equiv 1/2\rho U_\infty^2$
Re_c	Reynolds number based on chord
s	wing semispan length, b/2
s'	width of the unswept wing (s'=0.6096 m)
S_{ref}	reference surface area
$u_{p,j}$	peak velocity at ZNMF actuator slot exit
U, V, W	velocity components aligned with model coordinate system
U_∞	average freestream velocity
x_{sp}	distance from actuator to trailing edge

*Research Scientist, Flow Physics and Control Branch, Associate Fellow AIAA

x, y, z	coordinate system aligned with model leading edge
α	angle of attack, degrees
δ_f	flap deflection angle, degrees
Λ	sweep angle, degrees ($\Lambda = 30°$)
Λ'	$\arctan(\tan\Lambda\cos\alpha)$
Ω	Vorticity, $\frac{\partial W}{\partial x} - \frac{\partial U}{\partial z}$
ξ/c_R	x normalized by chord and rotated
ψ/c_R	z normalized by chord and rotated
ρ	density

A. Subscripts

R	Rotation of coordinate system to align model with camera angle

B. Abbreviations

2D	two dimensional
3D	three dimensional
AFC	active flow control
AR	aspect ratio
BART	Basic Aerodynamics Research Tunnel
LaRC	Langley Aeronautics Research Center
PIV	particle image velocimetry
SLA	stereolithography
SWJ	sweeping jet
ZNMF	zero net mass flux

I. Introduction

In this paper we present and discuss the use of active flow control (AFC) to delay separation that occurs at pre-stall angles of attack when the trailing edge flap of a 30° swept wing model is deflected. Active separation control on trailing edge flaps is of interest because it is a critical component of an AFC-enabled or simplified high lift system. A simplified high lift system that relies on AFC to meet performance goals is a technology that may be part of the Next Generation Air Transportation System (NexGen). This research, funded by NASA's Fixed Wing Project, contributes to their goal of advancing technologies that have the potential to improve the performance (reduce noise, reduce fuel burn, etc.) of future vehicles used for commercial transport.

An AFC-enabled high lift system was shown by McLean et al.[1] to be lighter, more streamlined, and require fewer parts than a conventional high lift system. Weight reduction is one of the major benefits of an AFC enabled high lift system. McLean et al.[1] surveyed various places on a commercial transport where active flow control could be applied. The replacement of the conventional trailing edge fowler flap with a hinged flap coupled with AFC for separation control was considered a high payoff application of AFC technology. Key elements needed to apply the technology were actuator efficiency and the ability to control separation on simple, hinged flaps with flap deflection angles greater than 30°, the typical flap deflection angle of most commercial transports during landing. Efficient application of flow control under these conditions requires that one have an understanding of the actuation being applied and the separated flowfield being controlled.

Zero net mass flux (ZNMF) actuators have been used in many flow control applications because studies[2–4] have shown that the periodic excitation produced by the actuators can be a very efficient (in terms of momentum) method of controlling separation. The efficiency of the method when using reduced frequencies of order 1 is attributed to the excitation generating 1 to 2 spanwise coherent vortices over the separated region. The vortices enhance the mixing between the separated shear layer and the low momentum flow near the model surface. ZNMF actuators were used in previous tests involving the current model by Greenblatt and Washburn.[5] The excitation, generated by external electromagnetic actuators, was introduced through

narrow slots, directed nearly tangential to the surface. The results showed that trailing edge flap separation could be reduced when using AFC on the unswept model, but when sweep was introduced and the model flap deflection angle was at its maximum, there was a small improvement on the inboard portion of the model and little to no improvement beginning near the middle of the model span. Since the excitation was introduced externally from one side of the model there was a concern that the excitation was not uniform along the span. In this set of experiments, we modified the model to test different actuator concepts to explore methods of improving AFC effectiveness over the span of the model.

Due to the challenge of developing small ZNMF actuators suitable for laboratory experiments with the required output for separation control, fluidic actuators are being used more often in flow control studies. While the actuators require an external pressure source, they have a very simple design and are easy to manufacture. Gregory and Tomac[6] provide a review of the fluidic actuator that describe the history of the device, including its current use as a flow control actuator. The fluidic actuators used in this investigation are termed sweeping jet actuators because there is no diverter at the actuator exit therefore the jet exiting the actuator sweeps from side to side. Vatsa et al.[7] performed a combined computational and experimental study that described the flowfield produced by this type of actuator. Koklu and Melton[8] documented the flowfield produced by the actuator using hotwire and particle image velocimetery measurements. They also looked at various output modes of the sweeping jet including the inclined jet that is produced when the feedback tubes of the actuator are blocked.

Fluidic actuators have proven effective in controlling flow separation thereby improving the performance of trucks,[9] bluff bodies,[10] airfoils, wings, and most recently a full-scale, vertical tail[a]. Seele et al.[11,12] used sweeping jet (SWJ) fluidic actuators to control separation on the rudder of a generic 12% thick vertical tail with a sweep angle of 42^o in a research effort aimed at reducing the drag due to the tail. They reported a 50% improvement in side force using C_μ levels below 2%. They also performed an extensive parameter study to optimize spacing and actuator location. DeSalvo et al.[13] used fluidic actuators on a 2D model and showed large improvements in lift. They used multiple slot locations and optimized the actuator exit design to reduce the C_μ levels needed to attach the flow to the flap of their model.

In this paper we describe the results obtained when using sweeping jet actuators to control separation on the trailing edge flap of a 15% thick model with a leading-edge sweep angle of 30°. Data are presented at flap deflection angles, δ_f, of 20°, 30°, and 40°. The majority of the paper is focused on the $\delta_f = 40°$ case. At $\delta_f = 40°$, PIV data are presented to aid in determining the effects of sweeping jet flow control on the off-body flowfeld.

II. Experiment Description

A. Wind Tunnel Description

The experiments were conducted in the NASA Langley Research Center (LaRC) Basic Aerodynamics Research Tunnel (BART). This open-circuit tunnel has an 11:1 contraction ratio and a test section that is 0.71 meters (m) high by 1.02 m wide by 3.05 m long. The maximum velocity of the tunnel is approximately 60 m/s. The freestream turbulence levels in the facility are less than 0.1% at this condition. BART is used primarily as a flow physics facility; therefore, it has the instrumentation and optical access needed for measurement techniques such as Laser Doppler Velocimetry (LDV) and PIV. Additional information about the wind tunnel can be found in Ref. 14. Most of the data that will be presented were acquired at a Reynolds number of 500,000 that corresponds to a freestream velocity of 25 m/s and a freestream Mach number of 0.07.

B. Model Description

The model tested is a semispan wing with a NACA 0015 cross-section normal to the leading edge that was built for sidewall AFC testing in the BART facility.[5,15,16] The model has a chord (c) that is 0.3048 m and a semispan (s) that is 0.68 m. The 30% constant chord trailing edge flap of the model can be tested at flap deflection angles, δ_f, from -10° to 40° in 10° increments. The 0.6096 m wide flap is divided into three 0.2032 m wide components that can be deflected independently. The original model was designed so that the effects of sweep on AFC could be studied. The swept configuration is achieved by inserting a 30°

[a] http://aviationweek.com/awin-featured-story/boeing-nasa-test-active-flow-control-tail

wedge between the unswept model and the endplate as shown in Fig. 1. The original unswept model had four rows of streamwise pressure taps at spanwise (y/s) locations of 0.17, 0.5, 0.83, and 0.99 and four rows of spanwise pressure taps at streamwise (x/c) locations of 0.005, 0.3, 0.705, and 1.0. The chordwise rows of static pressure orifices are normal to the leading edge of the model, as shown in Fig. 1(c), so they are not aligned in the streamwise direction when the model is swept. The C_p distributions that will be presented are computed in the manner described by Greenblatt and Washburn in Ref. 5. A left-handed coordinate system aligned with the model is used throughout the paper.

As had been done previously, the model was tested without boundary layer transition devices on the leading edge. The model was built with a 0.5 mm slot at the leading edge that was not used during this experiment. The authors in Ref. 5 concluded that the presence of the slot effectively tripped the boundary layer because of favorable comparisons between their baseline data using the unswept configuration and higher Reynolds number data on a different model. They did not perform studies to determine where transition occurred. Due to the fact that the unused leading edge slot was sealed during the portion of the experiment when actuators were located on the flap, sublimating chemicals were used to determine where transition occurred on the upper surface with and without the leading edge slot sealed. This study was done at a flap deflection of $\delta_f = 40^\circ$ where the majority of the data were acquired. The results of the transition study indicate that the leading edge slot does trip the boundary layer. With the slot sealed transition occurs slightly downstream of the slot at approximately 10% chord with the model angle of attack (α) at 6°. We sealed the gap between the deflected flap and the 30° wedge and did not add tip extensions to the model for the data that will be presented.

The second version of the General Aviation Circulation Control balance (GACC-2) was used to measure forces and moments for these experiments. The GACC-2 balance is a 5-component strain gage balance built for 2D, low-speed circulation control experiments in which the models are mounted vertically. Force and moment data in previous AFC experiments[5] using this model were obtained by integrating model surface pressures. The balance was added to improve the force and moment measurements and eliminate the need to retain the original number of pressure orifices on the SWJ actuator parts that were manufactured for this experiment. With the balance, surface static pressure measurements are not necessary to obtain force and moment data, but the measurements are beneficial in determining the effects of AFC, especially on this swept wing model.

C. SWJ Flap Actuators

The original trailing edge flap of the model[5] was replaced with a new flap manufactured using stereolithography (SLA). The flap was built in two parts that were bonded together to form one continuous part. An array of sweeping jet actuators were incorporated into the new flap design (Fig. 1(b)). The actuators were aligned parallel to the leading edge, located near the flap leading edge, and spaced $\Delta y/s' = 4.17\%$ (0.0254 m) apart in the y direction. The actuators are inclined at an angle of 35° to the flap surface. The actuator spacing, orientation, and location were influenced by the work of Woszidlo et al.[17] where the authors performed a parametric study of the sweeping jet actuator using a 2D model comparable in size to the current 3D model. They showed that the optimal spacing of the actuators was in the range of .0254 m (1 inch) to 0.0381 m (1.5 inch).[17] They also found that the excitation near the leading edge of the flap was effective at controlling separation on the flap of their model. The sweeping jet actuators we are using are scaled versions of the one described in Ref. 8. The width to height ratio of the orifice of each of the 23 actuators is 1:1. The orifice of each actuator is 1 mm wide and 1 mm high. The frequency of oscillation of a sweeping jet actuator depends on actuator geometry and the flow rate of the supply. Therefore, the actuators used in this experiment oscillate at frequencies in the kilohertz (KHz) range compared with the lower frequency range (75 Hz to 375 Hz) for the actuator used in Ref. 8. One inlet is used to supply air to the 23 sweeping jet actuators that cover the 0.6096 m width of the flap. Mass flow is measured by a mass flow meter inserted in the air supply line during wind tunnel testing. U_{jet} is computed using isentropic relations that rely on cavity pressure and temperature measurements from bench top testing. C_μ is calculated using the measured mass flow and computed U_{jet} values.

As discussed in the previous section, the new flap is instrumented with fewer static pressure orifices than the original flap. The center of the flap has more pressure orifices than the other y locations. Two rows of static pressure orifices at x/c=0.705 and x/c=1.0 are omitted as is the row of orifices at y/s'=0.99. The number of static pressure orifices was reduced to accommodate the SWJ actuator supply line that exits the model endplate through an existing opening sized for the original pressure instrumentation.

D. SWJ Upstream Actuators

In addition to manufacturing a new flap with sweeping jet actuators, new parts with SWJ actuators were made that could be inserted immediately upstream of the flap (Fig. 1(d)). The SLA-manufactured flap was replaced with the original flap when using these actuators so that more surface pressure data could be obtained. Unlike the SWJ flap actuators, the upstream actuators, located at the flap shoulder, can be replaced without removing the model from the tunnel. This feature reduces the time and cost to vary parameters such as actuator size and spacing. The height of the actuators was reduced to 0.5 mm so that the actuators could fit into the upstream region (Fig. 2(a)). The upstream SWJ actuators were built in three parts that are equal in width to the three flap sections of the original model. Each section of the upstream SWJ actuators had its own air supply line, regulator, and flowmeter.

We selected the actuator design used in Ref. 8 for this set of experiments because of the large sweep angle and therefore large region of influence of this type of sweeping jet when compared to a non-oscillating jet. The results of Koklu and Melton[8] and Vatsa et al.[7] show that in addition to the large sweep angle of the jets, the RMS velocity levels of the sweeping jets are on the order of the jet velocity for an actuator 6.25 times the size of the ones used in this study. Because the jet exiting the actuator spends less time in the center and more time near the maximum sweep angle, the average velocity profile of the larger version of this actuator has a double-peak with the peaks located on both sides of the centerline of the actuator.[7,8] The smaller actuators of this study do not seem to produce sweeping jets that have the same characteristics. Characterization of the actuators is challenging due to the small size of the upstream actuators and due to the fact that the sweeping jet flap actuators are bounded by a wall on one side. Hotwire and surface unsteady pressure measurements for the flap shoulder actuators along with the sound of the sweeping jet actuators confirm that the jets were oscillating. Oil flow data used to visualize the region of influence of each upstream sweeping jet actuator are shown in Fig. 2(b). The oil flow image is an average therefore it does not show the instantaneous motion of each of the jets. Each individual actuator in the array upstream and on the flap oscillates independently.

E. Particle Image Velocimetry

A stereoscopic PIV system comprised of a pulsed Nd:YAG laser operated at 10 Hz, two 2048 pixel x 2048 pixel cameras with camerlink interfaces, and acquisition software developed by Wernet[18] was used to acquire the PIV data. Two 150 mm macro lenses were used with the cameras, providing a field of view of 120 mm x 120 mm. The data were processed using commercially available PIV analysis software.[19] The interrogation window was 24 pixels x 24 pixels (1.36 mm x 1.36 mm) with an overlap of 50%. The PIV region is shown in Fig. 1(c). The cameras were located on the side of the tunnel opposite the turntable and rotated so that the flap surface was horizontal in each camera view. For our camera arrangement, the maximum total angle that could be set between the cameras was approximately 40°. Most of the PIV data were acquired at y/s'=0.52 to the right of the centerline row of pressure taps when looking downstream as shown in Fig. 1(c). This location is between two sweeping jet actuators on the flap of the model. The flowfield was seeded with 1 micron particles produced by a theatrical smoke generator. For the data presented, at least 600 image pairs were used to compute the mean values. Stereoscopic PIV was necessary because optical access is limited by the tunnel frame that divides the forward and aft regions of the BART test section near where the flap is located. The PIV data were acquired with the flap deflected to 40° and the model angle of attack set at 6°. The upper edge of the field of view of the upstream camera was slightly blocked by the tunnel frame.

III. Results

A. Control Using Zero-Net-Mass-Flux Actuator at $\delta_f = 20°$

Prior to using sweeping jet actuators, we used internal ZNMF electromagnetic actuators to control separation on the flap of the model. Internal actuators were mentioned as a follow on activity by the authors in Ref. 5. The reason for this recommendation is that internal actuators improve the uniformity of the excitation, a problem described in Ref. 5 due to using external actuators connected to one side of the model. The ZNMF flow control studies using internal, electromagnetic actuators were done with the model at a flap deflection of $\delta_f = 20°$. The ability of the ZNMF actuation to reattach the flow on the flap surface is illustrated in Fig. 3. The PIV data, shown for this flap deflection, were acquired using a similar PIV system to the one used in the

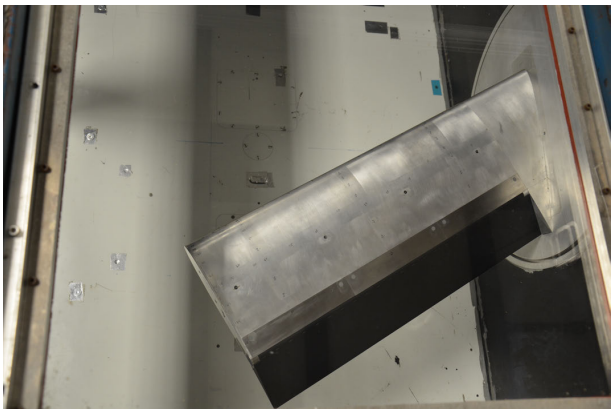

(a) **30° swept wing model installed in BART (view is looking down on model, through tunnel glass ceiling).**

(b) **SLA flap with sweeping jet actuators.**

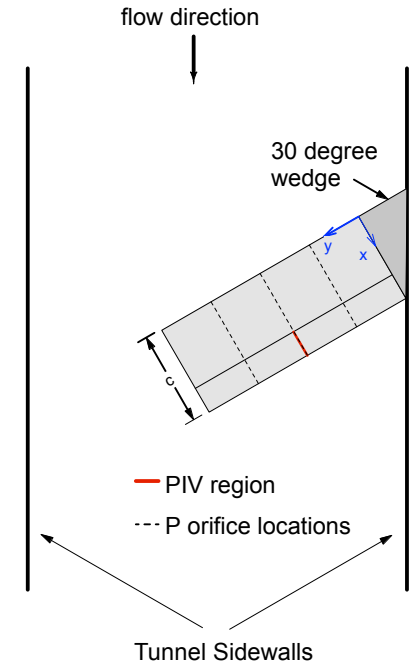

(c) **Sketch of model with PIV region highlighted.**

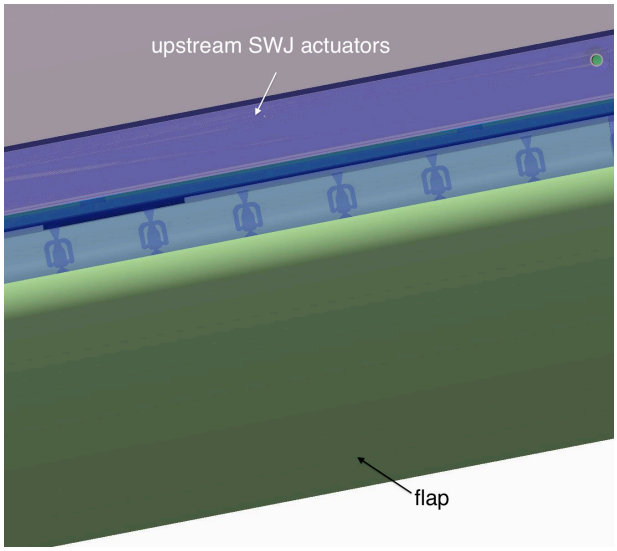

(d) **CAD image of trailing edge flap region of model with upstream sweeping jet actuators installed.**

Figure 1. Model installation in NASA LaRC BART facility.

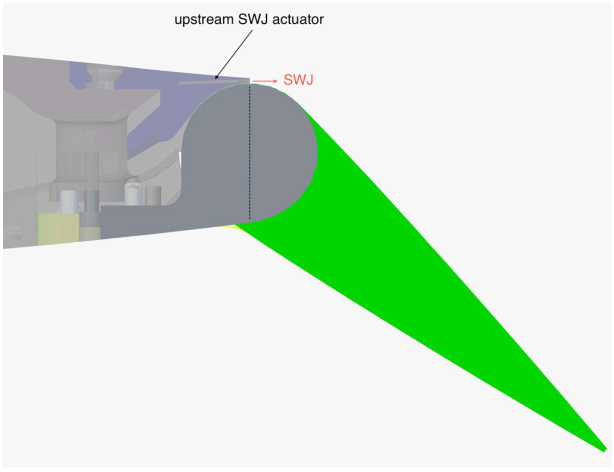

(a) **Side view of model flap region with upstream actuator installed.**

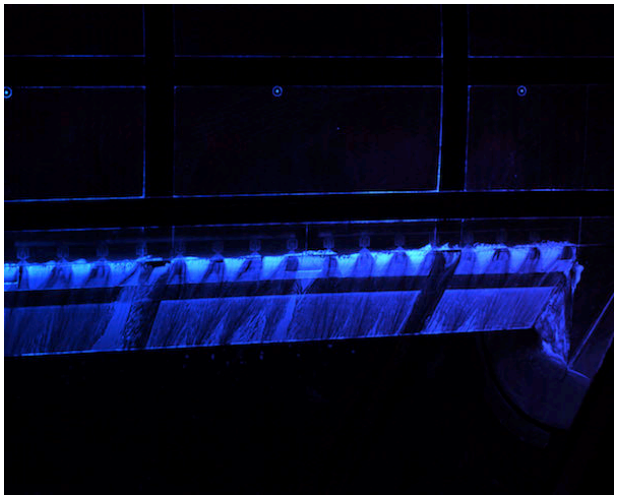

(b) **Oil flow visualization of the flowfield produced by sweeping jet actuators located upstream of the flap, U_∞=0.**

Figure 2. Upstream actuator location and flow visualization of the sweeping jets.

present study and described in section II E. When operating the actuators near their maximum operating conditions there was still a small amount of reversed flow near the trailing edge of the flap. Although not shown, other reduced frequencies were also studied and the results presented are representative of the improvements to the flowfield due to internal ZNMF AFC. While promising, these results point to the need for additional actuation to aid in controlling separation at higher flap deflection angles with larger adverse pressure gradients. The sweeping jet actuators used in the present study are an attempt at using a different type of actuator to obtain the control authority needed to reattach the separated flow on the flap.

In the sections that follow, results are presented for the case with sweeping jet actuators on the flap of the model to control separation. Surface static pressure distributions and lift data are used for flap deflection angles of 20° and 30° to evaluate the changes to the flowfield due to AFC. At δ_f=40°, PIV data are included with the C_p distributions and lift data to illustrate how the SWJ actuation affects the flowfield over the flap. Finally, data are presented for the case when excitation is introduced at the trailing edge flap shoulder using the upstream actuator. This is the same location used for the ZNMF AFC studies.

B. Control using SWJ Flap Actuators at $\delta_f = 20°$ and $\delta_f = 30°$

Figure 4(a) presents the lift increment obtained when using sweeping jet actuators with the flap at a deflection angle of 20°. The data show that lift increases for C_μ values less than 1.3% and the maximum lift increment for these C_μ levels is approximately 0.17. C_p distributions are presented in Fig. 4(b) for the baseline, no flow control case, and the C_p distribution has a plateau in the pressures on the flap upper surface indicating the flow is separated. The dotted line denotes the location of the flap hinge. For the three C_μ levels presented, AFC has an influence over a larger percentage of the flap as the level is increased. At a C_μ level of 1.28% there is significant amount of attached flow on the flap surface when compared to the baseline condition.

Figure 5(a) presents the lift increment obtained when using sweeping jet control with $\delta_f = 30^o$. With this larger flap deflection higher values of C_μ are required to reduce the amount of separated flow on the flap as compared to δ_f=20°. In addition to data at Re_c=500,000, data are also provided for Re_c=750,000 (U_∞=37 m/s, M=0.11). There is good overlap of the ΔC_L data for these two Reynolds numbers. The C_p distributions at y/s'=0.5 for select C_μ values are presented in Fig. 5(b). With the C_p data at this y/s' location, we see that at C_μ=2.59% the flow is almost completely reattached to the flap based on the fact that $C_p \approx 0$ at the trailing of the flap.

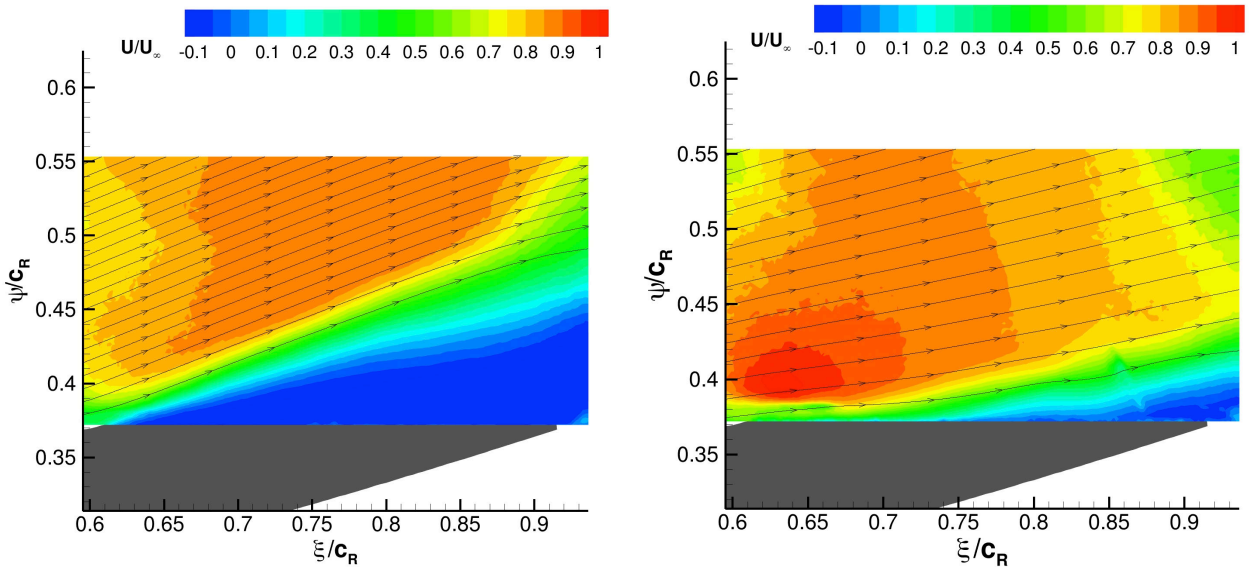

(a) **Baseline** (b) $C_{\mu,z} = 1.4\%$

Figure 3. Mean velocity contours with streamtraces overlaid from PIV data on the flap. Re_c**=500,000,** $\alpha = 6°$**,** $\delta_f = 20°$**.**

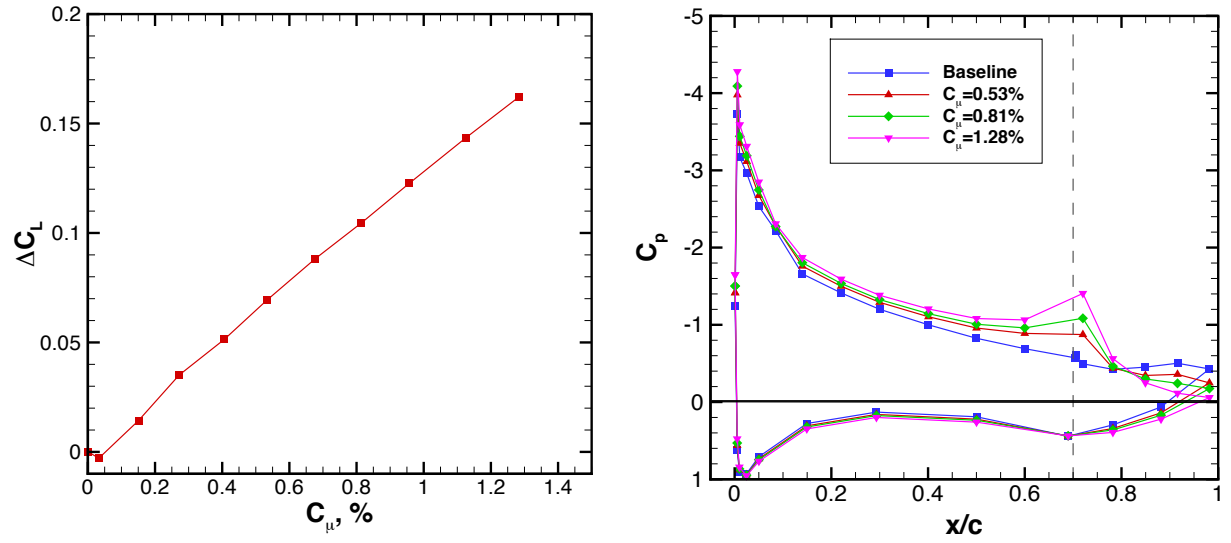

(a) **Lift Increment.** (b) C_p **distributions at** y/s'**=0.5.**

Figure 4. Lift increment due to varying C_μ **of SWJ flap actuator.** Re_c**=500,000,** $\alpha = 6°$**,** $\delta_f = 20°$**. Vertical dashed line represents flap hinge line.**

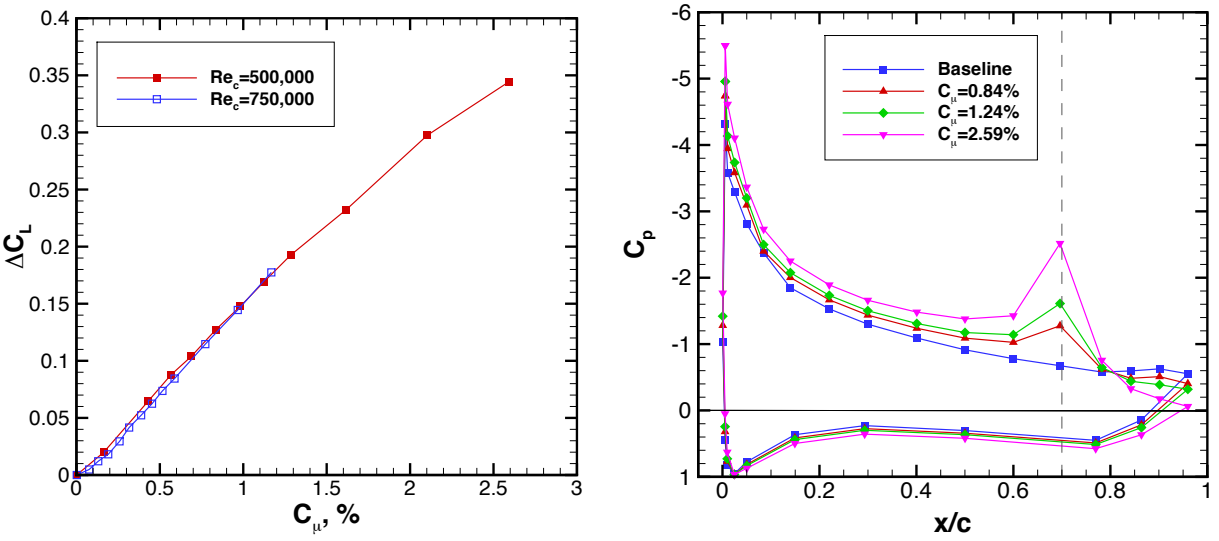

(a) **Lift Increment.** (b) C_p **distributions at** y/s'**=0.5.**

Figure 5. Lift increment due to varying C_μ **of SWJ flap actuator.** Re_c**=500,000,** $\alpha = 6°$**,** $\delta_f = 30°$**. Vertical dashed line represents flap hinge line.**

C. Control using SWJ Flap Actuators at $\delta_f = 40°$

Before presenting the AFC results with $\delta_f = 40°$, we present velocity and vorticity contours in Fig. 6 acquired using PIV that show the baseline flap flowfield. The data were acquired near y/s'=0.51 of the swept wing and 1200 image pairs were averaged to compute the mean values shown. These results show that at this flap deflection angle, the sweeping jets produced by the actuators are discharging into the separated flow field. Previous studies,[20] have shown that the ideal location for introducing control is upstream of the separation location. Although we will present results in the following sections that illustrate that the sweeping jet actuators in this configuration are capable of controlling separation, the location of the actuators is not optimal and more than likely results in higher C_μ levels being required to reattach the flow. The U velocity contours of Fig. 6(a) show that there is a large recirculation region on the flap surface. The excitation is introduced at ξ/c=0.64, downstream of where the flow separates. The V component of velocity is provided in the contour plot of Fig. 6(b) and show that the flow, in the direction parallel to the leading edge, on this 3D configuration is directed towards the tip of the model. At this location, the V component of velocity is positive over the model upper surface. Although not shown in Fig. 6(c), there is a small region of negative flow near ξ/c=0.93. The lack of separated flow in the y direction is used by Wygnanski et al.[21] as the reason to orient the sweeping jet actuators so that their exit axes are normal to the leading edge rather than in the streamwise direction. The reversal of the flow direction is noted in the W contours by the negative W values near the trailing edge of the model shown in Fig. 6(c). Finally, the vorticity contours in Fig. 6(d) show the location of the separated shear layer relative to the flap surface.

Data presented in Fig. 7 show the lift increment obtained when using the SWJ flap actuators with δ_f=40°. As mentioned previously, we sealed the leading edge slot of the model when using the flap SWJ actuators. For the C_μ values presented, we obtained a maximum increment in lift of 0.41. The pressure distributions, provided in Fig. 7(b) for the $y/s' = 0.50$ location, show that the flap sweeping jet control partially reattaches the flow to the flap of the model, increases the suction peak at the flap shoulder, and increases the suction pressures upstream of the flap. With larger values of C_μ, we reattached the flow to the flap at this Reynolds number even though the flap SWJ actuator array is not in the optimal location (i.e., it is downstream rather than upstream of separation).

In Fig. 8, contours of mean velocity and vorticity are shown for different values of C_μ. The data were acquired at y/s'=0.52, between two sweeping jet actuators, and 600 image pairs were averaged to compute the mean values presented. The velocity and vorticity contours illustrate the changes in the separated region on the flap as actuator momentum is increased. The data are shown with the model rotated to match the camera rotation angle. A C_μ level of 1.7% (Fig. 8(i)) delays separation to ξ/c_R=0.68 but there is still a large

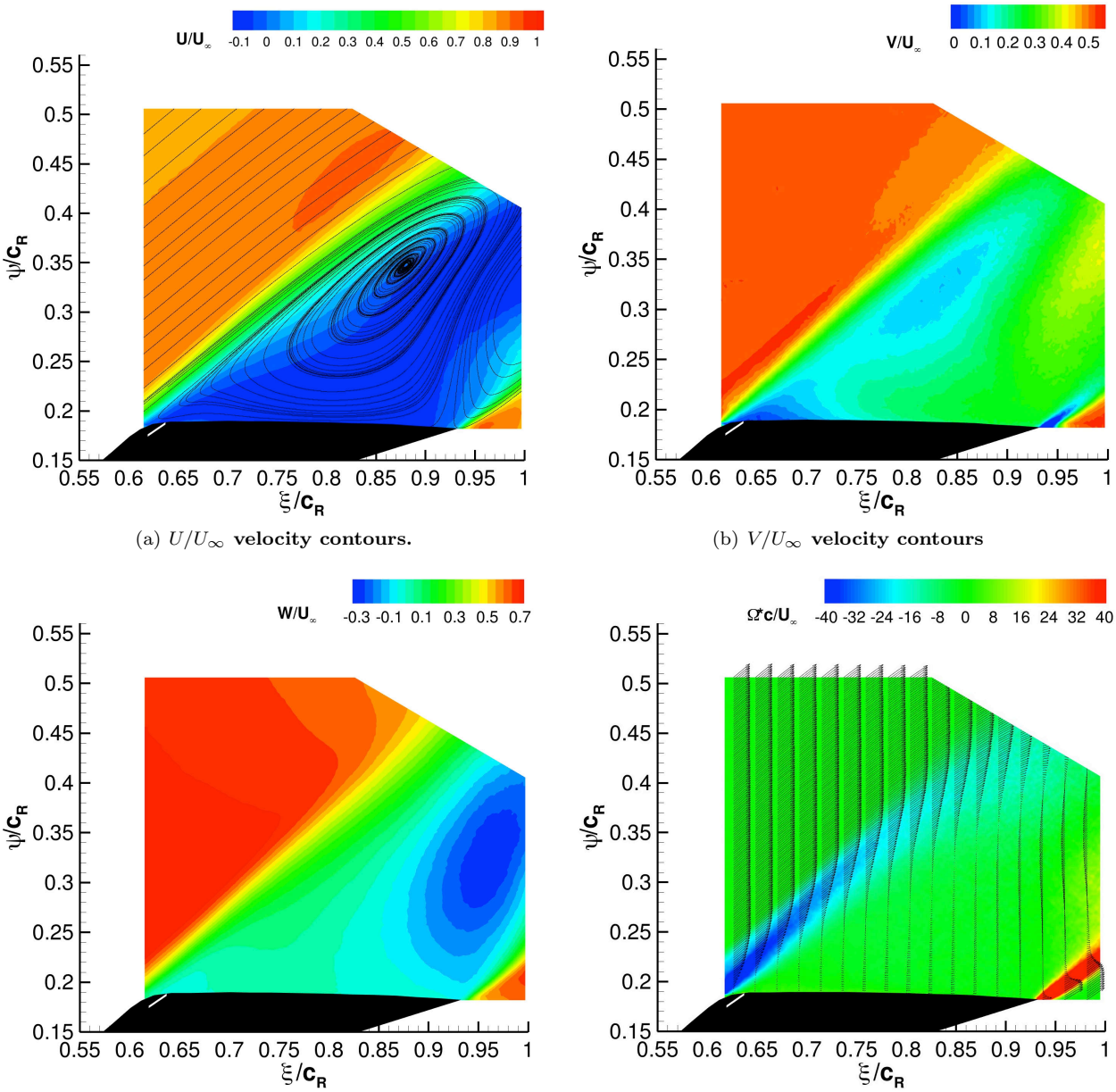

(a) U/U_∞ **velocity contours.**

(b) V/U_∞ **velocity contours**

(c) W/U_∞ **velocity contours.**

(d) **Vorticity contours.**

Figure 6. Contour plots from PIV data acquired on the trailing edge flap. Re_c**=500,000,** $\alpha = 6°$**,** $\delta_f = 40°$**.**

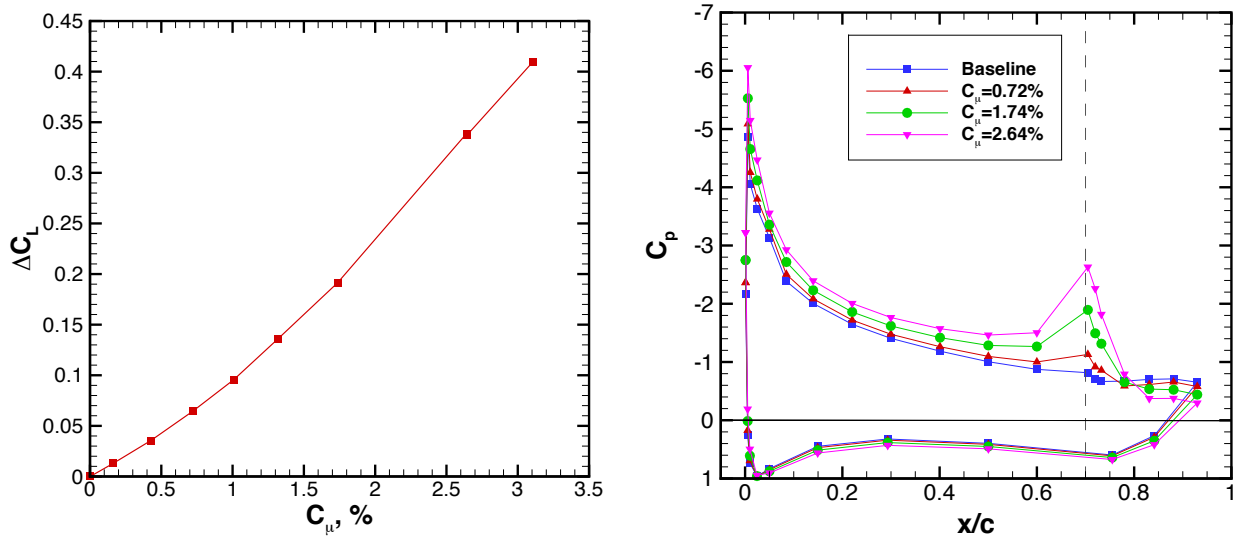

(a) **Lift Increment.** (b) C_p **distributions at** y/s'**=0.5.**

Figure 7. Lift increment due to varying C_μ **of SWJ flap actuator.** Re_c**=500,000,** $\alpha = 6°$**,** $\delta_f = 40°$**. Vertical dashed line represents flap hinge line.**

recirculation region on the flap. At C_μ=2.64% (Fig. 8(m)), separation occurs near ξ/c_R=0.72 and there is a smaller region of separated flow on the flap. At C_μ=3.1%, shown in Fig. 8(q), the flow separates near ξ/c_R=0.82 and there is a very small region of separated flow at the trailing edge of the flap.

Contours of the normalized velocity in the y direction, V/U_∞ are provide in Figs. 8(b), 8(f), 8(j), 8(n), and 8(r).The data show that with SWJ control, the out-of-plane component of velocity increases near the model surface resulting in more flow being directed toward the tip of the model. This is especially true of the data in Figs. 8(n) and 8(r) where the U and W components of velocity are near zero and the V component is approximately 50% of U_∞. At C_μ=2.64% (Fig. 8(n)), there are three distinct regions of low V velocity.

Contours of the normalized velocity in the z direction, W/U_∞, are provided in Figs. 8(c), 8(g), 8(k), 8(o), and 8(s). The data show lower values of W/U_∞ in the separated region compared to data in the freestream. The recirculation region directs a large amount of flow towards the trailing edge flap surface. This region becomes smaller as the recirculation region is reduced with increasing C_μ levels. For C_μ=2.64% (Fig. 8(o)) there are three regions centered at ξ/c_R=0.65, ξ/c_R=0.77, and ξ/c_R=0.93 where the velocity is a minimum on the flap of the model.

Vorticity contours are provided in Figs. 8(d), 8(h), 8(l), 8(p), and 8(s) and illustrate how SWJ control deflects the shear layer towards the flap surface as C_μ is increased and the separated region on the flap is reduced.

In Fig. 9, we present velocity and vorticity contours acquired using the mass flow rate needed to reattach the flow over the flap chord at y/s'=0.52. We include the data to complete the description of the reattachment process provided in Fig. 8. The U contours show that the velocity near the surface is positive(i.e, the flow is attached). The V contours of Fig. 9(b) indicate that the flow is directed toward the tip of the model. The local regions of low speed flow that were observed in Figs. 8(n) and 8(r) have been eliminated. The small region of low speed flow in the z direction at the trailing edge of the flap is no longer present (Fig. 9(c)). The SWJ excitation is responsible for the local region of low speed flow shown in Fig. 9(c) at ξ/c_R=0.65. With the flow reattached, the shear layer is on the flap surface (Fig. 9(d)).

D. SWJ Upstream Actuator Separation Control

The results with the upstream actuators, were obtained using sweeping jets with the same spacing, $\Delta y/s'$ =4.17%, as those on the flap. Due to the fact that the actuators could be located closer to the most inboard edge of the model, there are 24 actuators in this location. We tested three actuator configurations at this location. For the first configuration, we positioned the sweeping jets in the center of the part (Fig. 10(b)).

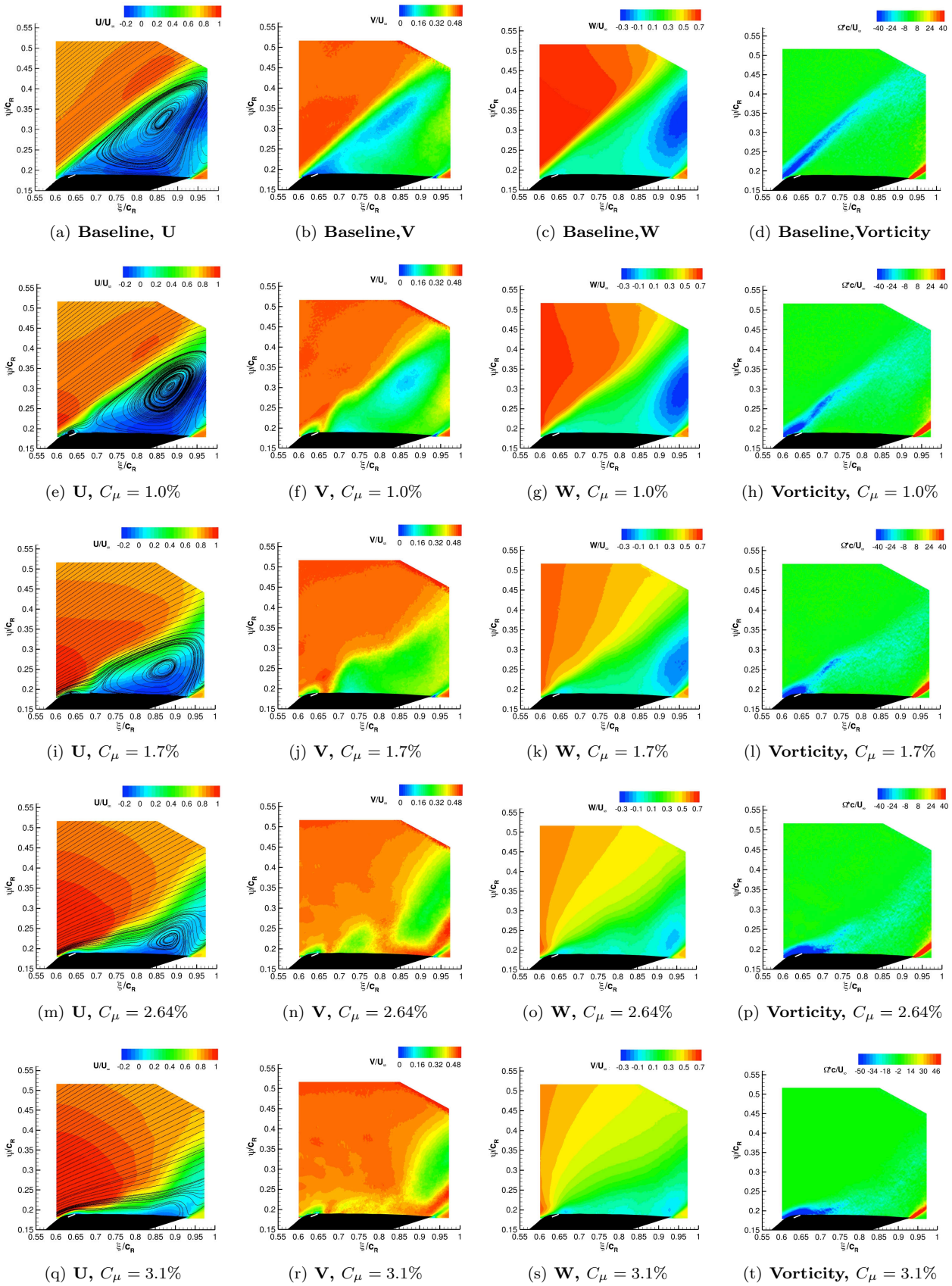

(a) **Baseline, U** (b) **Baseline,V** (c) **Baseline,W** (d) **Baseline,Vorticity**

(e) **U,** $C_\mu = 1.0\%$ (f) **V,** $C_\mu = 1.0\%$ (g) **W,** $C_\mu = 1.0\%$ (h) **Vorticity,** $C_\mu = 1.0\%$

(i) **U,** $C_\mu = 1.7\%$ (j) **V,** $C_\mu = 1.7\%$ (k) **W,** $C_\mu = 1.7\%$ (l) **Vorticity,** $C_\mu = 1.7\%$

(m) **U,** $C_\mu = 2.64\%$ (n) **V,** $C_\mu = 2.64\%$ (o) **W,** $C_\mu = 2.64\%$ (p) **Vorticity,** $C_\mu = 2.64\%$

(q) **U,** $C_\mu = 3.1\%$ (r) **V,** $C_\mu = 3.1\%$ (s) **W,** $C_\mu = 3.1\%$ (t) **Vorticity,** $C_\mu = 3.1\%$

Figure 8. Mean velocity and vorticity contours on the flap when using flap SWJ actuators. Re_c**=500,000,** $\alpha = 6°$**,** $\delta_f = 40°$**.**

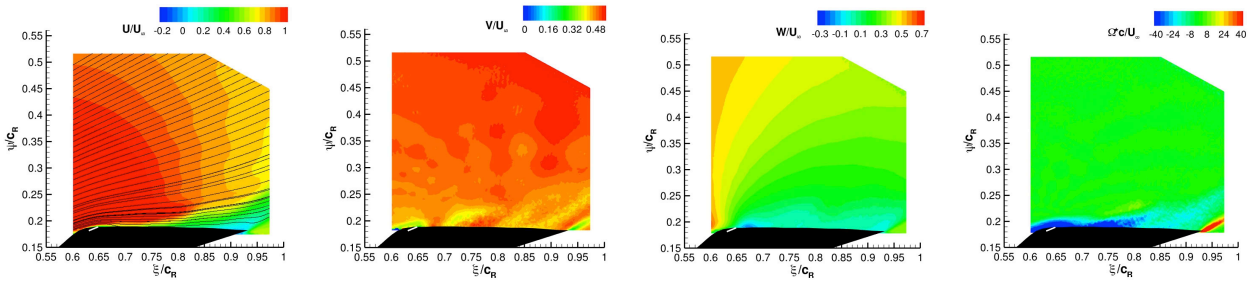

(a) **U** (b) **V** (c) **W** (d) **Vorticity**

Figure 9. Mean velocity and vorticity contours on the flap at needed to reattach flow SWJ using flap actuators. Re_c**=500,000,** $\alpha = 6°$**,** $\delta_f = 40°$**,** $\dot{m}$**=0.02 lb/s.**

For the second configuration, we increased the width of the actuator by 50%, which resulted in an actuator orifice aspect ratio of 3:1 versus the 2:1 aspect ratio used for the other two configurations. And in third configuration, we lowered the actuators in the part so that the jets exited directly onto the flap of the model (Fig. 10(c)). The third configuration was the most effective and is the one used for the results that will be presented. As mentioned previously, the original aluminum flaps were installed on the model when using these actuators and the leading edge slot was open.

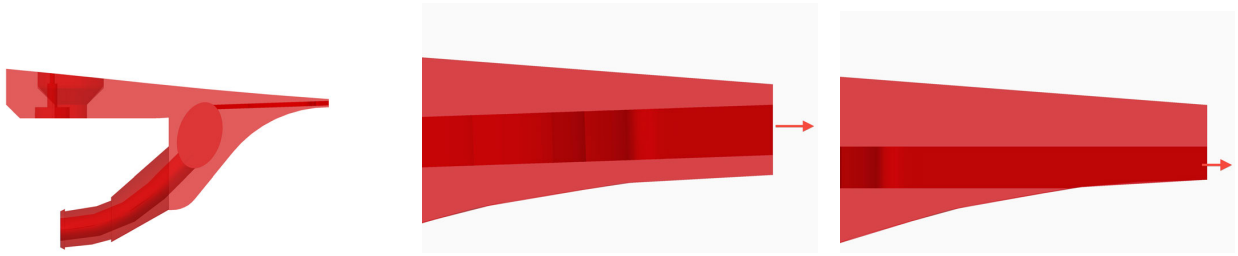

(a) **Upstream part with Configuration 1.** (b) **Close up view with actuators centered in the part at hinge line.** (c) **Close up view with actuators lowered in the part at hinge line.**

Figure 10. Upstream sweeping jet actuator vertical location.

Figure 11(a) presents the lift increments obtained when using the upstream SWJ actuators. Lift increment data when using the array of SWJ actuators on the flap are also included for comparison. The maximum increments in lift obtained using the upstream actuators for the C_μ levels shown is 0.40. For C_μ values up to 2.6%, less C_μ is needed to obtain the same lift increment using the upstream array of SWJ actuators compared to the C_μ values required when using the flap SWJ actuator array.

The C_p distributions provided in Figs. 11(b), 11(c), and 11(d) show how control affects the flow around the model at three y/s' locations. The baseline pressure distributions for all three cases show that the flow is completely separated on the flap. The pressure recovery on the flap, shown in Fig. 11(b), indicates that at y/s' a C_μ of 2.6% is effective at reattaching the flow to the flap. The baseline C_p distribution for the most inboard location, y/s'=0.17, does not have a slope of zero on the flap. PIV data acquired at this location and not shown indicated that the recirculation region at y/s'=0.17 is smaller when compared to the one at $y/s' \approx 0.5$. Sweeping jet control, at y/s'=0.17, does not produce the same pressure recovery over the flap when compared to the other two y/s' locations. Similar results with sweeping jet control at the most inboard location were noted by Seele et al.[12] who attributed the differences in the inboard flow control region to interaction of the SWJ control with the juncture flow vortex. Nonetheless, lift is increased at all three locations as evidenced by the pressure recovery, increase in suction at the flap shoulder, and the increase in circulation upstream of the flap.

This paper has primarily focused on the C_L increment obtained at a fixed angle of attack, $\alpha = 6°$. In Fig. 12 we provide data that show the lift coefficient over the angle of attack range investigated during the experiment for the baseline and four C_μ levels. The data show that the lift increments that have been presented for $\alpha = 6°$ are similar up to 12° where stall begins for the C_μ=2.6% case.

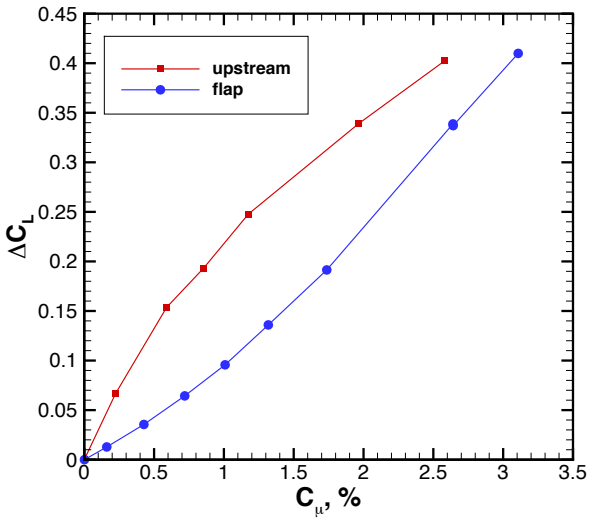

(a) **Lift Increment.**

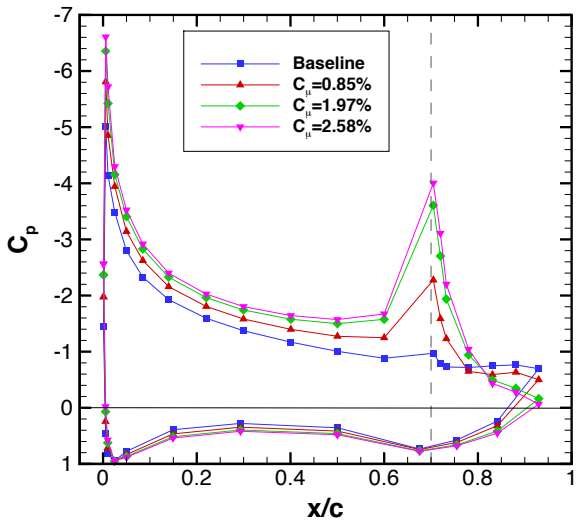

(b) C_p **at** y/s'**=0.50**

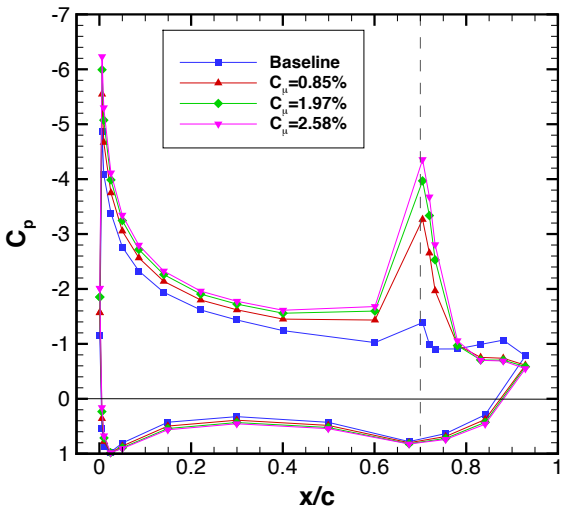

(c) C_p **at** y/s'**=0.17.**

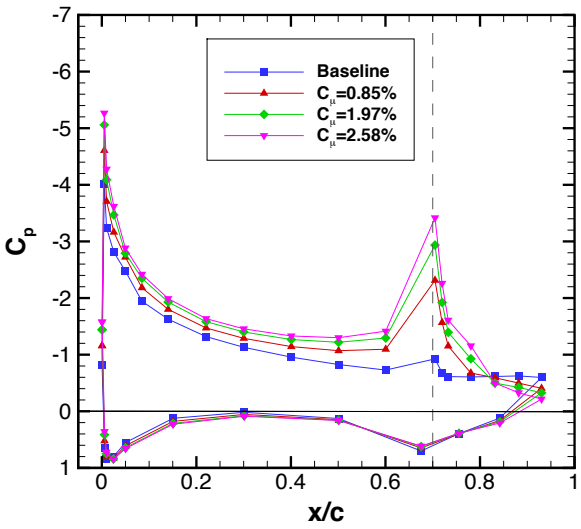

(d) C_p **at** y/s'**=0.83.**

Figure 11. Lift increment and C_p **distributions when using the upstream actuator.** Re_c**=500,000,** $\alpha = 6°$**,** $\delta_f = 40°$**. Vertical dashed line represents flap hinge line.**

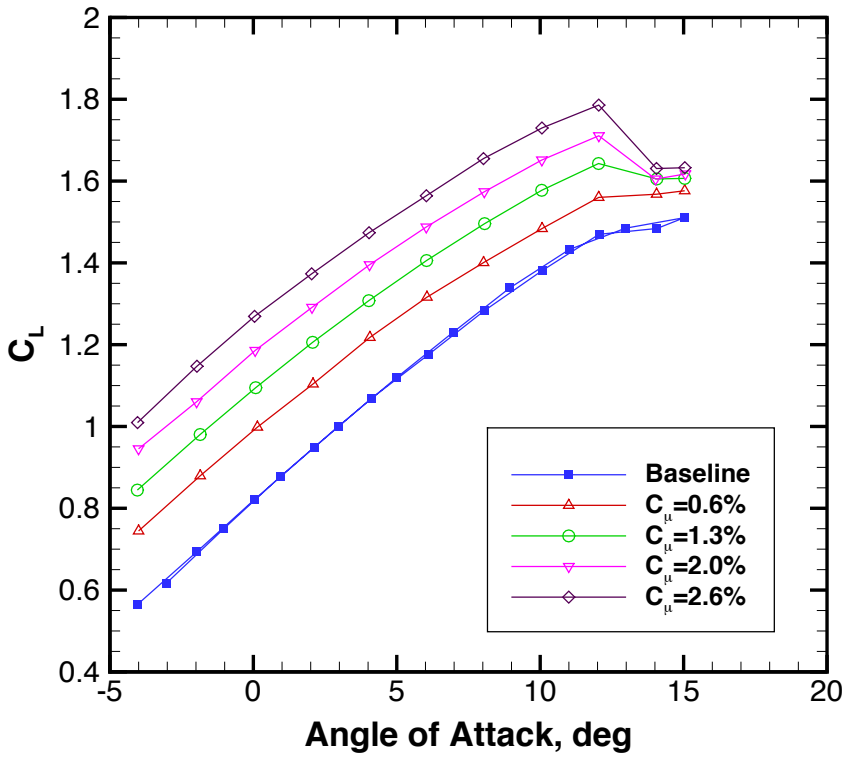

Figure 12. Lift coefficients for Re_c=500,000 and $\delta_f = 40°$.

IV. Summary

Active flow control using fluidic actuators in the form of sweeping jets was applied to the trailing edge flap of a 30° swept wing model with aspect ratio of 4.35 to control the separation that occurs when the flap is deflected. This configuration is being studied because of the potential benefits of flow control to reduce the complexity of the high lift system of commercial transports. Sweeping jet actuators were selected because they can provide the necessary control authority on this size model to control separation at the maximum flap deflection of 40 degrees and a Reynolds number of 500,000. While separation was controlled with the sweeping jet actuators used in this set of experiments, additional studies are needed to optimize the system so that the momentum requirements can be reduced. Future studies should use larger actuators, with width to height ratios of 1:1 or 2:1 to reduce the sweeping jet velocities thereby improving the efficiency of the actuation system. Other parameters that need to be investigated are actuator spacing and actuator frequency.

Acknowledgments

The authors would like to thank the Fixed Wing Project of the NASA Fundamental Aeronautics Program for funding the research and the following individuals for their support; Catherine McGinley, John C. Lin, Mehti Koklu, Judi Hannon, Norman Schaeffler, Greg Jones, Donald, Day, and Charlie Debro. Thanks are also extended to Chung-sheng Yao, Jerome Harris, and Luther Jenkins for help with the PIV acquisition and analysis. The authors also thank model designers Vincent LeBoffe and Sandy Webb for their work on the model support system, internal actuator design and sweeping jet integration. Thanks are extended to Tom Hall, Robert Andrews and Gary Wainwright for help with various aspects of the model fabrication process. Finally the authors thank Dan Neuhart and Lewis Owens for their expertise in helping to evaluate the state of the boundary layer using sublimating chemicals.

References

[1]McLean, J. D., Crouch, J. D., Stoner, R. C., Sakurai, S., Feifel, G. E., Feifel, W. M., and Rush, H. M., "Study of the Application of Separation Control by Unsteady Excitation to Civil Transport Aircraft," NASA/CR 1999–209338, 1999.

[2]Seifert, A. and Pack, L. G., "Active Flow Separation Control on Wall-Mounted Hump at High Reynolds Numbers," *AIAA Journal*, Vol. 40, No. 7, 2002, pp. 1363–1372.

[3]Seifert, A. and Pack, L. G., "Oscillatory Control of Separation at High Reynolds Numbers," *AIAA Journal*, Vol. 37, No. 9, 1999, pp. 1062–1071.

[4]Greenblatt, D. and Wygnanski, I., "The Control of Flow Separation by Periodic Excitation," *Progress in Aerospace Sciences*, Vol. 36, 2004, pp. 487–545.

[5]Greenblatt, D. and Washburn, A., "Influence of Finite Span and Sweep on Active Flow Control Efficacy," *AIAA Journal*, Vol. 46, No. 7, 2008, pp. 1675–1694.

[6]Gregory, J. W. and Tomac, M., "A Review of Fluidic Oscillator Development and Application for Control," AIAA Paper 2013-2474, 2013.

[7]Vatsa, V. N., Koklu, M., Wygnanski, I. J., and Fares, E., "Numerical Simulation of Fluidic Actuators for Flow Control Applications," AIAA Paper 2012-3239, 2012.

[8]Koklu, M. and Melton, L., "Sweeping Jet Actuator in a Quiescent Environment," AIAA Paper 2013–2477, June 2013.

[9]Seifert, A., Stalnov, O., Sperber, D., Arwatz, G., Palei, V., David, S., Dayan, I., and Fono, I., "Large Trucks Drag Reduction Using Active Flow Control," AIAA Paper 2008-0743, Jan. 2008.

[10]Wilson, J., Schatzman, D., Arad, E., Seifert, A., and Shtendel, T., "Suction and Pulsed-Blowing Flow Control Applied to an Axisymmetric Body," *AIAA Journal*, Vol. 51, No. 10, 2013, pp. 2432–2446.

[11]Seele, R., Graff, E., Gharib, M., Taubert, L., Lin, J., and Wygnanski, I., "Performance Enhancement of a Vertical Tail Model with Sweeping Jet Actuators," AIAA Paper 2013–0411, Jan. 2013.

[12]Seele, R., Graff, E., Gharib, M., Taubert, L., Lin, J., and Wygnanski, I., "Improving Rudder Effectiveness with Sweeping Jet Actuators," AIAA Paper 2012–417, June 2012.

[13]DeSalvo, M., Whalen, E., and Glezer, A., "High-Lift Enhancement using Active Flow Control," *AIAA 2011-3355*, June 2011, pp. 1–16.

[14]Sellers, W. and Kjelgaard, S., "The Basic Aerodynamics Research Tunnel- A Facility Dedicated to Code Validation," AIAA Paper 1988–1997, May 1988.

[15]Greenblatt, D., "Dual Location Separation Control on a Semispan Wing," *AIAA Journal*, Vol. 45, No. 8, 2007, pp. 1848–1860.

[16]Greenblatt, D., "Management of Vortices Trailing Flapped Wings via Separation Control," AIAA Paper 2005–0061, Jan. 2005.

[17]Woszidlo, R., Nawroth, H., Raghu, S., and Wygnanski, I., "Parametric Study of Sweeping Jet Actuators for Separation Control," AIAA Paper 2010–4247, July 2010.

[18]Wernet, M. P., "Fuzzy Logic Enhanced Digital PIV Processing Software," Tech. rep., 18th International Congress on Instrumentation for use in Aerospace Simulation Facilities, June 1999.

[19]Scarano, F. and Riethmuller, M., "Advances in Iterative Multigrid PIV Image Processing," *Experiments in Fluids Supplemental*, Vol. 29, 2000, pp. S51–S60.

[20]Melton, L. P., Yao, C., and Seifert, A., "Active Control of Separation from the Flap of a Supercritical Airfoil," *AIAA Journal*, Vol. 44, No. 1, 2006, pp. 34–41, previously AIAA Paper 2003–4005.

[21]Wygnanski, I., Tewes, P., and Taubert, L., "Applying the Boundary-Layer Independence Principle to Turbulent Flows," *Journal of Aircraft*, Vol. 51, No. 1, Jan. 2014, pp. 175–182.